Oblique and cellular vortex shedding behind a circular cylinder in a bidirectional shear flow

Zhiyong Huang,[1,2] Vagesh D. Narasimhamurthy,[1,a)] and Helge I. Andersson[1]
[1]*Department of Energy and Process Engineering, Fluids Engineering Division, Norwegian University of Science and Technology (NTNU), 7491 Trondheim, Norway*
[2]*Centre for Ships and Ocean Structures (CeSOS), 7491 Trondheim, Norway*

(Received 21 December 2009; accepted 11 June 2010; published online 15 November 2010)

Vortex shedding in the transitional wake of a circular cylinder in a shear flow has been investigated. The focus has been on the effect of a bidirectional shear, i.e., the oncoming unidirectional flow varied linearly both in the spanwise and cross-stream directions. The computer experiments showed that the bidirectional shear resulted in a wake with oblique and cellular vortex shedding similar to the cylinder wake resulting from spanwise shear alone. The presence of a planar shear, however, gave rise to longer cellular cells. Due to the bidirectional shear inflow, the pressure was higher along the high-velocity side of the cylinder surface than along the low-velocity surface and at the same time exhibited a spanwise variation, which gave rise to secondary motions along the stagnation line and in the base region. Even though the cross-stream shear component was four times larger than the spanwise shear, the latter tended to dominate the three-dimensional wake dynamics.
 [doi:10.1063/1.3483488]

I. INTRODUCTION

Flow past circular cylinders was probably the most studied bluff-body configuration during the past century.[1] Substantial progress has been made during the past two decades in the understanding of the wake transition and vortex instabilities behind a circular cylinder placed in a uniform inflow.[2–10] From their Floquet stability analysis, Barkley and Henderson[7] found that the wake transition, i.e., the spatial transition that renders the flow three dimensional, occurs already at Reynolds number 189. The experimental studies of Williamson[3] further revealed the presence of large-scale vortex dislocations, which are an intrinsic feature of the wake transition process. The successive stages of this laminar-turbulent transition, i.e., from a two-dimensional laminar vortex shedding to mode A shedding and from mode A shedding to mode B shedding, were discussed in great detail by Williamson.[9] The existence of this two-stage wake transition, first discovered in the experiments by Williamson,[2] was later observed in the direct numerical simulations (DNSs) of Zhang *et al.*,[4] Thompson *et al.*,[8] and Persillon and Braza.[10] The DNS data further reinforced and complemented the knowledge gained through laboratory experiments. Today, the wake transition of a circular cylinder placed in a uniform inflow is rather well understood.

In practice, however, the oncoming flow is rarely uniform. In nature, the atmospheric boundary layer and the seabed boundary layer exhibit a substantial mean shear. The local topography may also give rise to other asymmetries of the oncoming flow. Depending on the orientation of the mean shear flow with respect to the cylinder axis, two different flow configurations can arise, each producing completely different flow physics behind the cylinder. When the oncoming flow varies in the cross-stream direction, i.e., mean shear flow across the cylinder, the resulting flow exhibits asymmetric vortex shedding (see Refs. 11–16) and is popularly called *planar shear flow* [see Fig. 1(a)]. If, on the other hand, the oncoming flow varies in the axial or spanwise direction, i.e., mean shear flow along the cylinder span, the wake flow is known to exhibit oblique and cellular vortex shedding (see Refs. 17–25) and is popularly termed as *axial* or *spanwise shear flow* [see Fig. 1(b)]. Table I lists the various studies carried out on sheared flows past a circular cylinder. One can observe that both the planar shear flow and the spanwise shear flow have received rather modest attention from the research community in spite of their obvious practical relevance. DNS studies are particularly scarce.

If we now focus our attention on the planar shear case, it is very surprising to see that none of the studies so far has investigated the wake transition (see Table I). Even though Kiya *et al.*[11] performed experiments in the Reynolds number range of 35–1500, their measurements were limited to the Strouhal number and with high degree of uncertainty. They reported, however, that the temporal transition, i.e., transition from a steady state to an unsteady state, was delayed due to the presence of a planar shear. They concluded that the critical Reynolds number beyond which vortex shedding occurs was higher in their planar shear studies compared to the uniform inflow case. In direct contrast to their conclusion, more recently, Lankadasu and Vengadesan[26] found that with increasing shear, the onset of vortex shedding occurs at a lower Reynolds number compared to the uniform inflow case. In spite of this confusion, it is anyhow interesting to note that planar shear has an effect on the temporal transition. Unfortunately, no such information is available with respect to spatial or wake transition. Although Lei *et al.*[15] considered low Reynolds number flows, their computations were based

a)Author to whom correspondence should be addressed. Telephone: +47 73593563. Fax: +47 73593491. Electronic mail: vagesh@ntnu.no.

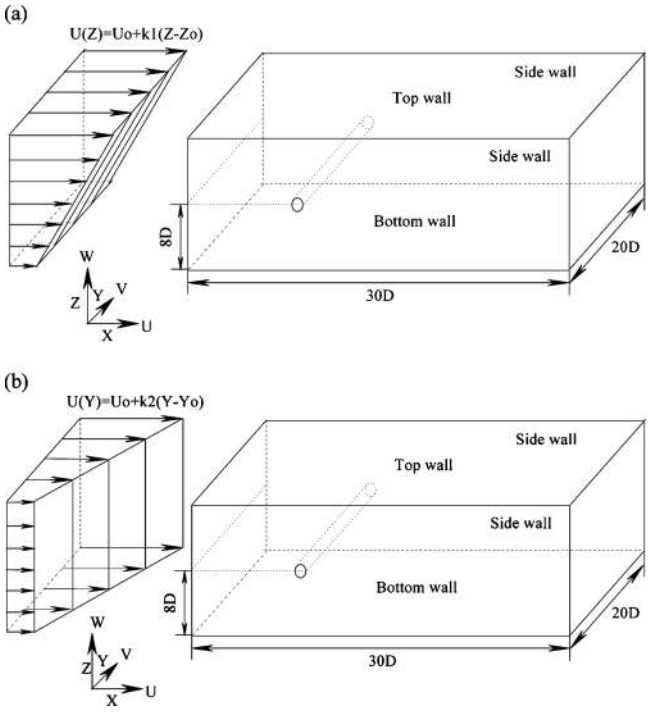

FIG. 1. Computational domain (not to scale) and coordinate system. The midpoint of the circular cylinder is at (X_o, Y_o, Z_o). (a) Planar shear case: $k1=0.1$, $k2=0$. (b) Spanwise shear case: $k1=0$, $k2=0.025$.

on two-dimensional (2D) Navier–Stokes equations and thus unable to adequately address the transition process.

In contrast to the planar shear case, the spanwise shear case has received much attention from the scientific community. In addition to mathematical modeling (see references cited in Refs. 24 and 22), experimental and DNS studies have been carried out (see Table I), although all the experiments fall in high Reynolds number turbulent regime. In a review paper, Griffin[17] summarized the observations made by earlier experiments. Oblique and cellular vortex shedding has been observed in all the experiments so far, while Rooney and Peltzer[20] and Woo *et al.*[21] reported spanwise variation of the base pressure. In addition, Woo *et al.*[21] also observed secondary flow in the base region. The DNS computations of Silvestrini and Lamballais[23] and Mukhopadhyay *et al.*[24,25] have also revealed the oblique and cellular vortex shedding behind circular cylinders. In addition, Mukhopadhyay *et al.*[24,25] reported both instantaneous and mean base pressure gradients along the span. In a recent article, Parnaudeau *et al.*[27] provided secondary flow data from the DNS computations of Silvestrini and Lamballais.[23] It is worth mentioning here that similar flow physics has been observed recently by Narasimhamurthy *et al.*[28,29] in the wake of a tapered circular cylinder. Apart from the wake transition study carried out by Silvestrini and Lamballais,[23] no more information is available in literature (see Table I) regarding transition in a spanwise shear inflow. A more detailed analysis of the wake dynamics, together with the Reynolds-averaged statistical data, is therefore awaited.

All the previous investigators have considered unidirectional shear flow past circular cylinders, i.e., either planar shear flow or spanwise shear flow. In nature, however, the oncoming shear is rarely unidirectional. The effect of bidirectional shear flow on the wake of a circular cylinder is therefore not clear at this stage. The present DNS study is

TABLE I. Various studies on sheared flows past a circular cylinder. Here Re_o refers to the Reynolds number based on the median velocity U_o and the diameter of the cylinder, while $k1$ and $k2$ are the shear parameters for the planar shear case and the spanwise shear case, respectively.

Authors	Method	Re_o	Flow regime	$k1$	$k2$
Present study	DNS	240	Transition	0.1	0.025
Kiya *et al.*[a]	Expt.	35–1500		0–0.25	
Kwon *et al.*[b]	Expt.	600–1600	Turbulence	0–0.25	
Sumner and Akosile[c]	Expt.	$(4-9)\times10^4$	Turbulence	0.02–0.07	
Cao *et al.*[d]	Expt.	10^4–5.5×10^4	Turbulence	0–0.27	
Lei *et al.*[e]	2D Num.	80–1000		0–0.25	
Omori *et al.*[f]	LES	3900	Turbulence	0–0.177	
Mair and Stansby[g]	Expt.	$(1.3-2.6)\times10^4$	Turbulence		0.012–0.048
Tavoularis *et al.*[h]	Expt.	$(1.7-2.5)\times10^4$	Turbulence		0.063–0.161
Rooney and Peltzer[i]	Expt.	$(2-4)\times10^5$	Turbulence		0.02–0.03
Woo *et al.*[j]	Expt.	$800-4\times10^4$	Turbulence		0.034
Kappler *et al.*[k]	Expt.	3.13×10^3–1.25×10^4	Turbulence		0.02, 0.04
Silvestrini and Lamballais[l]	DNS	200	Transition		0.025, 0.1
Mukhopadhyay *et al.*[m]	DNS	131.5	Laminar		0.02
Mukhopadhyay *et al.*[n]	DNS	131.5	Laminar		0.02

[a]Reference 11.
[b]Reference 12.
[c]Reference 13.
[d]Reference 14.
[e]Reference 15.
[f]Reference 16.
[g]Reference 18.
[h]Reference 19.
[i]Reference 20.
[j]Reference 21.
[k]Reference 22.
[l]Reference 23.
[m]Reference 24.
[n]Reference 25.

TABLE II. Flow parameters.

Case	AR	Re_o	Re_h	Re_l	$k1$	$k2$
Uniform inflow	20	240	⋯	⋯	⋯	⋯
Planar shear flow	20	240	⋯	⋯	0.1	⋯
Spanwise shear flow	20	240	300	180	⋯	0.025
Bidirectional shear flow	20	240	300	180	0.1	0.025

aimed to explore such a complex scenario, where a circular cylinder is subjected to a bidirectional shear flow in the wake transition regime. The bidirectional shear flow was generated by a combination of planar shear and spanwise shear profiles. For comparison, three DNS cases were considered, where the same circular cylinder is subjected to uniform inflow, planar shear inflow, and spanwise shear inflow, respectively. Data from both spectral analysis and instantaneous flow visualizations from each of the cases will be presented and compared. The spanwise variations of the velocity and the pressure fields will also be shown. Reynolds-averaged statistical quantities will be presented and the underlying physics will be highlighted.

II. FLOW CONFIGURATION AND NUMERICAL METHOD

Let us consider the flow past a circular cylinder with the view to explore the effects of various inflow conditions on the vortex shedding. The flow configuration is shown in Fig. 1. Four different flow cases were considered, namely, the uniform inflow, the planar shear flow, the spanwise shear flow, and finally a combination of planar shear and spanwise shear flow giving rise to a bidirectional shear flow case. The flow parameters concerning the four different cases are shown in Table II. The aspect ratio of the cylinder $AR=l/D=20$, where l is the length of the cylinder and D is the diameter. The median Reynolds number Re_o based on the median velocity U_o (i.e., inflow velocity at $X=0$, $Y=10D$, $Z=8D$) and the diameter of the cylinder is 240 in all the four cases. Due to the substantial variation of the inflow velocity in the spanwise shear case and the bidirectional shear case, the local Reynolds number $\mathrm{Re}=UD/\nu$ varies from 180 to 300 along the span (here U is the local inflow velocity along the span). The Reynolds number at the high- and low-velocity ends are defined as $\mathrm{Re}_h=U_hD/\nu$ and $\mathrm{Re}_l=U_lD/\nu$, respectively (here U_h and U_l are the inflow velocities at the high- and low-velocity ends, respectively). Thereby, the Reynolds number range chosen in the present DNS study is such that both the mode A and the mode B transitional flow regimes may coexist along the span of the cylinder. In the planar shear flow case [see Fig. 1(a)] the dimensionless shear parameter $k1$ is defined as $k1=AD/U_o=0.1$, where $A=\partial U/\partial Z$ is the velocity gradient of the inflow in the cross-stream direction. Similarly, the dimensionless shear parameter $k2$ in the spanwise shear flow case [see Fig. 1(b)] is defined as $k2=BD/U_o=0.025$, where $B=\partial U/\partial Y$ is the velocity gradient of the inflow in the spanwise direction. In the present article, all spatial dimensions are normalized by D and all velocities are scaled with the median velocity U_o, unless otherwise explicitly mentioned.

The Navier–Stokes equations in incompressible form were solved in three-dimensional space and time using a *parallel* finite-volume code called MGLET.[30] The code uses staggered Cartesian grid arrangements. Discretization of the spatial derivatives was achieved by means of a second-order central-differencing scheme. The momentum equations are advanced in time by a fractional time stepping using a third-order explicit Runge–Kutta scheme. For the Poisson equation, Stone's incomplete lower-upper (LU) decomposition method (strongly implicit procedure) was used. The size of the computational domain in each coordinate direction was $L_x=30D$, $L_y=20D$, and $L_z=16D$, as shown in Table III. The cylinder axis was positioned at $X_o=10D$ and $Z_o=8D$, while $Y_o=10D$ being the center of the cylinder span. The cross-stream domain width $16D$ is not sufficiently large to make blockage effects totally negligible (see, e.g., Ref. 31) but our

TABLE III. Domain size and grid parameters from various uniform inflow (Refs. 4, 8, and 10) and spanwise shear inflow (Refs. 24, 25, and 23) studies.

Case	Re_o	L_x	L_y	L_z	N_x	N_y	N_z
Present DNS	240	30	20	16	384	192	192
Zhang *et al.*[a]	180–300	22	9	12	144	60	144
Thompson *et al.*[b]	200–250	16	3.14	7	⋯	⋯	⋯
Persillon and Braza[c]	100–300	54	2.25	32	213	15	102
Mukhopadhyay *et al.*[d]	131.5	15	24	15	80	120	80
Mukhopadhyay *et al.*[e]	131.5	15	48	15	80	240	80
Silvestrini and Lamballais[f]	200	22	48	12	397	385	216

[a]Reference 4.
[b]Reference 8.
[c]Reference 10.
[d]Reference 24.
[e]Reference 25.
[f]Reference 23.

TABLE IV. Present results compared against data available to date in literature. Re=300 in all the cases. St, θ, and λ_B are Strouhal number, separation angle, and wavelength of mode B, respectively.

Case	St	θ	λ_B	C_{pb}
Present result	0.214	110	0.75	−1.19
Zhang *et al.*[a]	0.212	⋯	≈1.0	⋯
Barkley and Henderson[b]	⋯	⋯	0.82	≈−1.2
Persillon and Braza[c]	0.206	106.5	0.70	−1.378
Williamson and Roshko[d]	≈0.203	⋯	⋯	≈−0.96
Norberg[e]	≈0.203	⋯	⋯	≈−1.0

[a]Reference 4.
[b]Reference 7.
[c]Reference 10.
[d]Reference 34.
[e]Reference 35.

L_z nevertheless compares favorably with the domain widths used in many related studies. Among the entries in Table III, only Persillon and Braza[10] used a wider domain. With the aim to compare the wake resulting from the four different inflow cases listed in Table II, the modest blockage effects can be assumed to be the same in all the cases considered. The number of grid points in each coordinate direction ($N_x \times N_y \times N_z$) was equal to $384 \times 192 \times 192$, respectively. Non-equidistant grid spacings were used in the X-Z plane, while an equidistant grid was used along the span (Y-direction). The ratio of grid size Δ near the cylinder to the diameter is $\Delta/D=0.02$. The spanwise grid spacing $\Delta Y \approx 0.10D$ is probably not sufficient to capture the very tiniest details associated with the vortex dislocations observed for instance by Williamson.[3] Nevertheless, flow visualizations of the vortex shedding behind a tapered plate by Narasimhamurthy *et al.*[33] exhibited an overwhelming fine structure in spite of a spanwise grid spacing of about 0.12 of the mean plate width. From Table III, it is clear that the present grid resolution is much finer than what has been used in most other DNS studies and compares favorably with that of Silvestrini and Lamballais.[23] The time step was chosen as $\Delta t=0.002D/U_o$. The computations were performed on an IBM P575+ parallel computer.

At the inlet, velocity profiles were prescribed without any free-stream perturbations and a Neumann boundary condition was used for the pressure. A free-slip boundary condition was applied on both side walls, as well as at the top and bottom walls. At the outlet, a Neumann boundary condition was used for velocities and the pressure was set to zero. A direct forcing immersed boundary method[32] was used to transform the no-slip condition at the cylinder surface into internal boundary conditions at the nodes of the Cartesian grid. The internal boundary condition value had to be determined by interpolation. In the present study, we used least-squares interpolation of third-order accuracy. The detailed derivation, validation, and implementation of this technique in the code MGLET were explained in Ref. 32 and its versatility demonstrated recently by Narasimhamurthy *et al.*[33]

Before undertaking this study, a benchmark DNS calculation of the uniform flow past a circular cylinder at Reynolds number 300 was carried out. This simulation was performed on a shorter domain size of $L_x \times L_y \times L_z$ equal to $20 \times 6 \times 16$, i.e., on a shorter aspect ratio cylinder. The results were found to be in good agreement with the data available in the existing literature (see Table IV). The differences observed in the base pressure coefficient C_{pb} values when compared to the experiments[34,35] are due to the short aspect ratio cylinders used in the simulations when compared to the very high aspect ratios used in experiments.

III. RESULTS AND DISCUSSION

A. Wake pattern and frequency analysis

The time evolution of the instantaneous velocity components U, V, W, and the instantaneous pressure P were sampled along a line parallel to the axis of the cylinder and located $2D$ downstream the axis in the X-direction and offset by $1D$ in the Z-direction. The total sampling time was equal to $80D/U_o$, which covers about 15 vortex shedding cycles. The spatiotemporal pattern from both the uniform inflow case and the planar shear case indicated parallel vortex shedding, i.e., vortices were shed parallel to the axis of the cylinder. The time traces of the cross-stream velocity W for the spanwise shear case and the bidirectional shear case are shown in Figs. 2(a) and 2(b), respectively. Here, the wake pattern clearly indicates *oblique* and *cellular* vortex shedding with random occurrence of *vortex dislocations* or

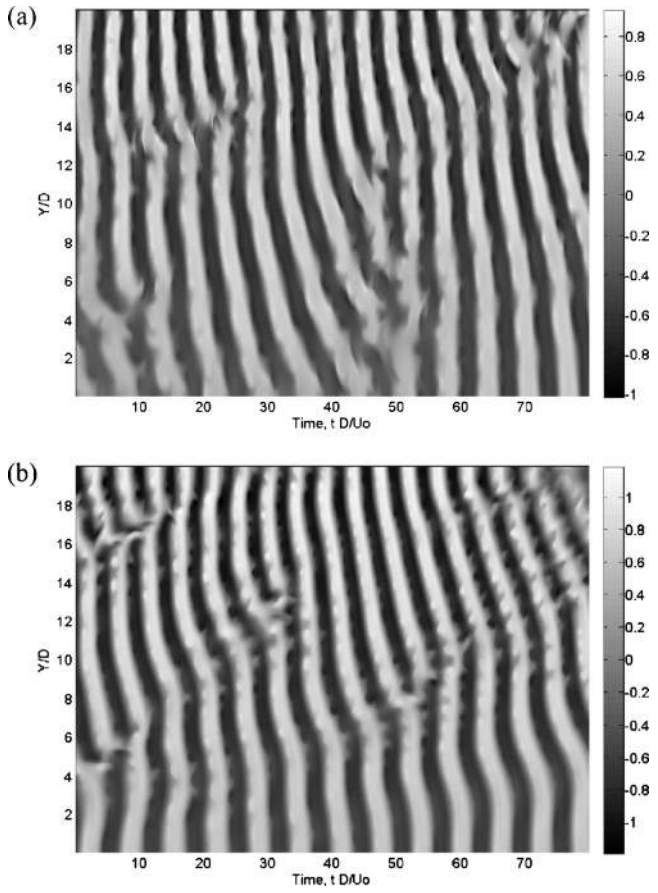

FIG. 2. Time evolution of the cross-stream velocity (W) showing vortex dislocations along the entire span. The sampling line is at $X/D=2$ and $Z/D=1$ (measured from the axis of the cylinder). $Y/D=0$ corresponds to $Re_l=180$ and $Y/D=20$ corresponds to $Re_h=300$: (a) spanwise shear and (b) bidirectional shear.

vortex splits along the span. Spatiotemporal plots from Mukhopadhyay *et al.*[25] and Parnaudeau *et al.*[27] also indicate such transient aspects of the cellular shedding, where the vortex dislocations are not appearing periodically at the same spanwise location. Such a cellular pattern, which is decorrelated in time, was also observed recently by Narasimhamurthy *et al.*[29] in the wake of a tapered circular cylinder. In the absence of mean shear flow, vortex dislocations in the transitional wake of a circular cylinder are known to occur during the changeover of eddy shedding mode from laminar to mode A and from mode A to mode B.[2,3]

In order to make quantitative comparisons between the wake patterns of the four cases considered, frequency spectra were analyzed by carrying out Fourier analysis of the cross-stream velocity W time traces. In the uniform inflow case, the Strouhal number $\mathrm{St}=fD/U_o$ (where f is the shedding frequency) obtained from the fast Fourier transform of the velocity signal was equal to 0.204 and therefore in good agreement with the experimental data.[3] Kiya *et al.*[11] in their planar shear flow study found that in the Reynolds number range of 100–1000 and for $k1>0.1$, the Strouhal number increased with the increasing shear parameter. Kwon *et al.*[12] also came to similar conclusions from their experiments in the Reynolds number range of 600–1600. However, in the recent experiments of Sumner and Akosile[13] and Cao *et al.*,[14] they observed that the shear parameter $k1$ had no significant influence on the Strouhal number at subcritical Reynolds numbers. The apparently contradictory findings in earlier studies of vortex shedding in planar shear flow arise since the vortex shedding is not only determined by the oncoming shear rate $k1$ and the Reynolds number but also by the blockage ratio of the actual cylinder as well as of the cylinder aspect ratio. On the basis of the present simulations, where the Strouhal number for the planar shear case was 0.185, we are inclined to conclude that a modestly sheared inflow, i.e., $k1\leq 0.1$, tends to reduce the Strouhal number.

In Fig. 3(a), the Strouhal number data from both the spanwise shear case and the bidirectional shear case are plotted along the span. Note that the shedding frequency is varying along the span in discrete steps between cells of constant shedding frequency. The distinct contrast in the cellular pattern between the two cases is evident. Note that the bidirectional shear case ($k1=0.1$, $k2=0.025$) considered here is essentially a spanwise shear flow ($k2=0.025$) superimposed on a planar shear flow ($k1=0.1$). Therefore, the differences in the cellular pattern in Fig. 3(a) are due to the presence of planar shear component in the bidirectional shear case. It can be inferred from Fig. 3(a) that the addition of planar mean shear to the spanwise shear flow leads to fewer and longer cells. Nevertheless, it is at least interesting to see the variations in the cellular structure, although the overall variations are confined to approximately the same Strouhal number range of $0.15<\mathrm{St}<0.23$.

If we now compare the Strouhal number data from the present spanwise shear case with the Silvestrini and Lamballais,[23] it can be observed that the Strouhal number variation from about 0.15 to 0.23 along the span almost coincides with that found in Ref. 23, although the actual vortex

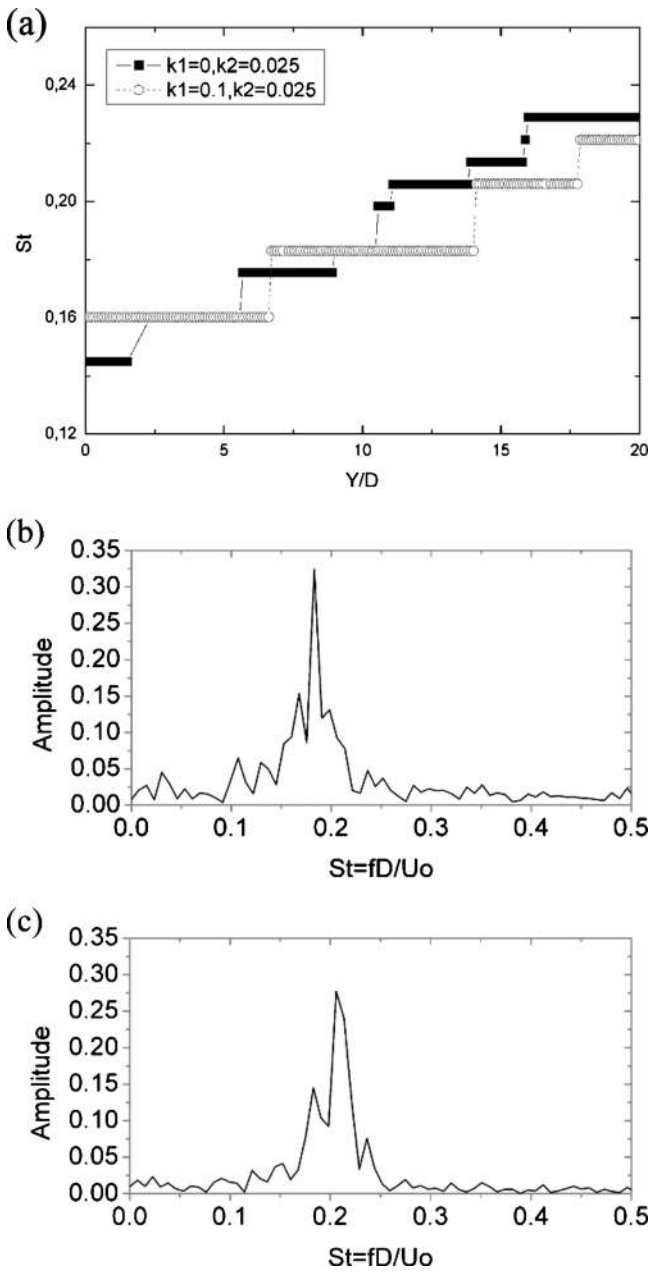

FIG. 3. (a) Strouhal number $\mathrm{St}=fD/U_o$ along the span from both the present spanwise shear case (■) and the bidirectional shear case (○). $Y/D=0$ corresponds to $\mathrm{Re}_l=180$ and $Y/D=20$ corresponds to $\mathrm{Re}_h=300$. [(b) and (c)] Local velocity spectra from the bidirectional shear case evaluated at $Y/D=10$ and $Y/D=16$, respectively.

cell splitting occurs at different spanwise locations. Please remember that the shear parameter $k2$ in both the present study and in Silvestrini and Lamballais[23] is the same (see Table I). In addition, both studies were carried out in the wake transition regime. However, the reason for this small deviation in the cellular pattern lies in the fact that different aspect ratios (AR) were used in the two cases (see Table III). Due to their long cylinder ($AR=48$), the Reynolds number of Silvestrini and Lamballais[23] varied from 100 to 300, thereby accommodating both the laminar and the transition regimes along the span of their cylinder. The present study, however, comprised only the wake transition regime ($180<\mathrm{Re}<300$). The presence of different flow regimes and aspect

ratio variations are known to alter the cellular vortex shedding pattern. Recently, Narasimhamurthy *et al.*[29] observed cellular shedding behind a tapered circular cylinder in the wake transition regime, where the Reynolds number along the span varied from 100 to 300. However, a direct comparison of the Strouhal number data between the two cases is not possible. This is because in the uniform flow past a tapered cylinder, the high frequency side along the span corresponds to low Reynolds number flow and the low frequency side corresponds to high Reynolds number flow (see, e.g., Ref. 29). This is in contrast to the spanwise shear case, where the high frequency side corresponds to high Reynolds number and low frequency side corresponds to low Reynolds number flow (see Ref. 27 for more differences between the two cases). In spite of this, the Strouhal number variations along the span in the Reynolds number range of 180–300 in the present spanwise shear case and in Ref. 29 were approximately in the same range.

B. Instantaneous vortical structures

An essential distinction between the spanwise shear inflow and the planar shear inflow cases should be pointed out. The former case is associated with a uniform incoming vorticity ω_z in the cross-stream direction. This vorticity is being stretched due to $\omega_z \partial w/\partial z$ and tilted due to $\omega_z \partial u/\partial z$ in the vicinity of the cylinder. The tilting of the vortex tubes results in streamwise-oriented vorticity. At least to a first approximation, such vortex stretching and tilting mechanisms are not occurring in the case of a planar shear inflow, in which the oncoming spanwise vorticity ω_y is altered only by advection and diffusion.

In order to study the vortical structure information, the spanwise vorticity component ω_y and the enstrophy or vorticity magnitude $|\omega|$ were analyzed. Isocontours of ω_y and $|\omega|$ from all the four cases are shown in Figs. 4 and 5, respectively. The distinct contrast between the shedding patterns in the four cases is striking. Three dimensionalities in the form of waviness in the spanwise vortex cores (primary Karman vortices) are evident in all the four cases. In Figs. 4(a) and 4(c), i.e., in the present uniform inflow case and the planar shear case, the Reynolds number $\mathrm{Re}_o = 240$ is constant along the whole span. Williamson[9] in his review article reported that in the Reynolds number range of 230–260, a gradual transfer of energy takes place from mode A shedding to mode B shedding. In addition, both experiments and simulations have predicted that the two modes of instability (A and B) can coexist in this Reynolds number interval. If we now look into Figs. 5(a) and 5(c), the snapshots show the appearance of small-scale streamwise structures along the span. The corresponding wavelength indicates predominantly mode B instabilities with few mode A streamwise structures occurring at some places. The top and side views of the planar shear flow in Figs. 4(c) and 4(d) reveal a distinct asymmetric vortex shedding. While the wake is symmetric about the X-axis in the uniform inflow case [see Fig. 4(b)], the vortex street is shifted toward the low-velocity side in the planar shear case in Fig. 4(d). Such an asymmetric shedding was also observed in the low Reynolds number experiments

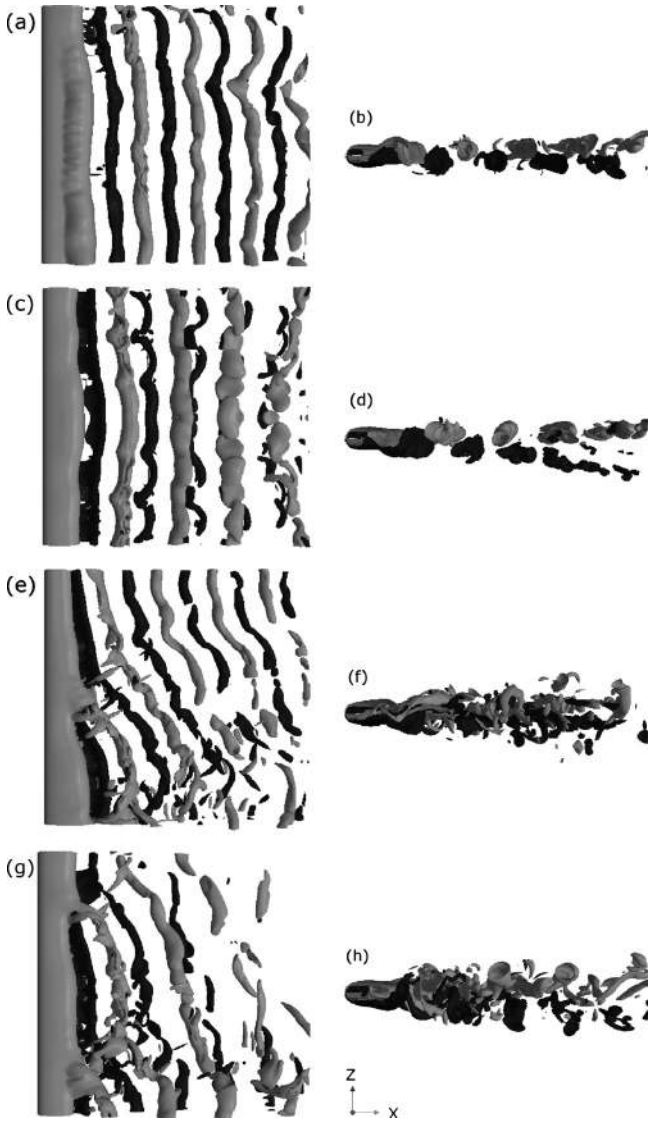

FIG. 4. Three-dimensional isocontours of spanwise vorticity ω_y. The isocontour level is the same in all the plots. Dark and light colored surfaces represent negative and positive ω_y, respectively: [(a) and (b)] uniform inflow, [(c) and (d)] planar shear, [(e) and (f)] spanwise shear, and [(g) and (h)] bidirectional shear.

of Kiya *et al.*[11] and the high Reynolds number large-eddy simulations (LES) of Omori *et al.*[16] A similar deflection of the vortex street was reported by Kieft *et al.*[31] in their study of the wake structure behind a heated cylinder and by Khaledi *et al.*[36] for a normal plate wake in a rotating environment. These vortex-street deflections can be ascribed to the difference in strength between the two vortex rows.

The tilting of the vortex street in the present study is partly a direct consequence of the gradually increasing inflow velocity with Z. The planar shear inflow is equivalent to a uniform spanwise vorticity $\Omega_y = \partial U/\partial Z > 0$, which corresponds to a clockwise rotation of the fluid elements. The imposed vorticity Ω_y interacts differently with the spanwise vorticity ω_y generated along the upper and lower cylinder surfaces. It can be observed that the anticlockwise Karman vortices shed from the low-velocity side of the cylinder is weak and more irregular than the clockwise vortices shed

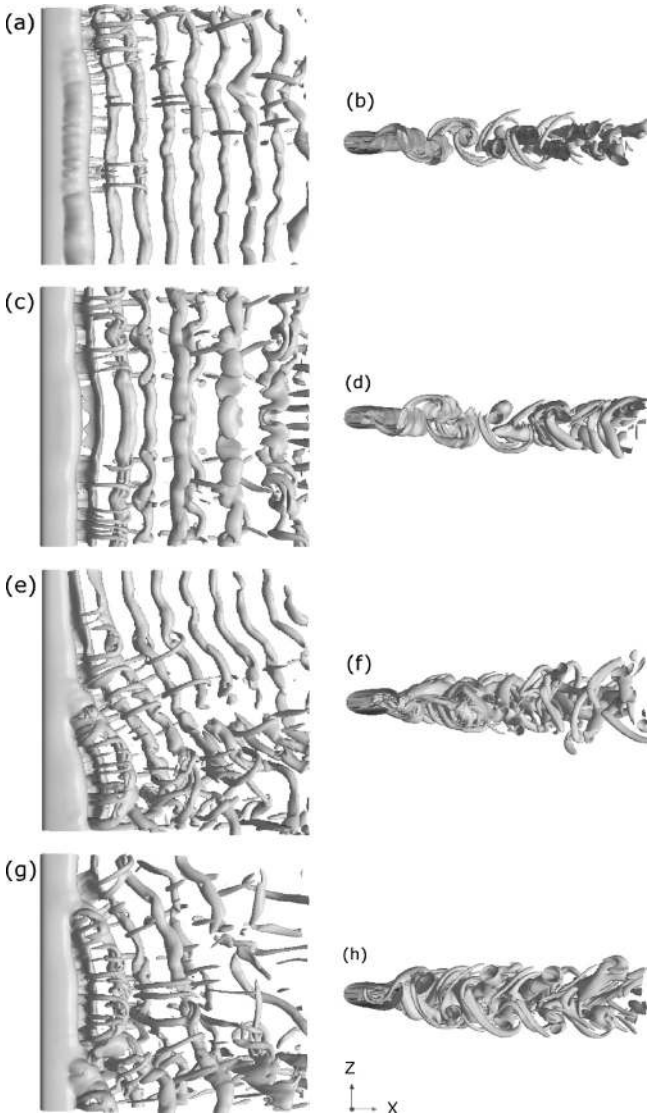

FIG. 5. Three-dimensional isocontours of enstrophy or vorticity magnitude $|\omega|$. The isocontour level is the same in all the plots: [(a) and (b)] uniform inflow, [(c) and (d)] planar shear, [(e) and (f)] spanwise shear, and [(g) and (h)] bidirectional shear.

from the high-velocity side. Since the vorticity generated in the boundary layer along the low-velocity side of the cylinder is of opposite sign of the uniform vorticity Ω_y associated with the inflow, the planar shear flow tends to weaken the Karman cells shed from the lower side. The Karman vortices shed from the high-velocity side are shed into a mean vorticity field of the same sign and the shed cells are not adversely affected. If we compare the shedding pattern in Figs. 4(a) and 4(c), it can be inferred that the presence of planar shear enhances the three-dimensionality in the form of wavy distortion of the spanwise rolls.

The vortex dislocations formed between spanwise cells of different frequencies when the primary vortices become out of phase with each other are visible in Figs. 4(e) and 4(g), i.e., in the present spanwise shear case and the bidirectional shear case, respectively. The development of helical twisting of vortex tubes is visible in the vicinity of the vortex dislocations. Williamson[3] concluded that these helical twistings are the fundamental cause for the rapid spanwise spreading of dislocations, and, indeed, for the large-scale distortion and breakup to turbulence in the wake transition behind a circular cylinder. The vortices first starts to shed from the high-velocity end [lower part of Figs. 4(e) and 4(g)], which corresponds to $\mathrm{Re}_h=300$, and therefore sheds at an angle to the axis. The flow visualizations in both experiments[21,22] and in DNS computations[25,23] revealed such oblique and cellular shedding. If we compare the shedding pattern in Figs. 4(e) and 4(g), it can again be inferred that the addition of planar shear to the spanwise shear inflow causes large-scale wake distortions and thereby enhances the three-dimensionality in the wake transition process. Due to the substantial variation of the local Reynolds number along the span (from 180 to 300) in Figs. 5(e) and 5(g), i.e., in the present spanwise shear case and the bidirectional shear case, respectively, both modes of instability (mode A and B) coexist along the span. Again in Fig. 5(g), large-scale vortex distortion downstream of the cylinder is strikingly visible when compared to the spanwise shear case in Fig. 5(e). The combination of two types of shear, thus, successfully promotes the wake three-dimensionality and eventually leads to early break-up to turbulence.

C. Mean pressure coefficient and secondary motion

The mean pressure coefficient is defined as $C_p=2(\bar{P}-P_\infty)/(\rho U_o^2)$, where the reference pressure P_∞ is taken from the pressure at the inflow. The distribution of C_p on the surface of the cylinder from both the present uniform inflow case and the planar shear case is shown in Fig. 6(a). The current base pressure coefficient at the rearmost location ($\theta=180°$) for the uniform inflow case is -1.0, which is in good agreement with the experimental value of -0.92 from Williamson and Roshko.[34] For a slightly lower Reynolds number than in the present study, i.e., at $\mathrm{Re}_o=200$, the DNS computations of Persillon and Braza[10] and Thompson *et al.*[8] predicted the base pressure coefficient equal to -1.05 and -1.25, respectively, as compared to the experimental value of -0.85 from Williamson and Roshko.[34] Persillon and Braza[10] argued that their too short span ($AR=2.25$) was the cause for this discrepancy. The present base pressure coefficient, however, is in good agreement with the measurements and this observation suggests that the present cylinder span $AR=20$ is adequate.

C_p in the planar shear case is higher than that for the uniform inflow case along the high-velocity side and lower along the low-velocity side up to θ about 70° [see Fig. 6(a)]. This is probably associated with the shifting of the front stagnation point toward the high-velocity side, as discussed by Lei *et al.*[15] and Cao *et al.*[14] Thereafter, C_p values on the two sides collapse along the after-body, i.e., downstream of the separation region. The same observations were also made in the experiments of Sumner and Akosile[13] and in the LES simulations of Omori *et al.*[16] However, the base pressure coefficient in the present planar shear case is slightly lower than that in the uniform inflow case. This is in contrast to both the experimental[13,14] and LES data,[16] where the base pressure was significantly higher than that in their corre-

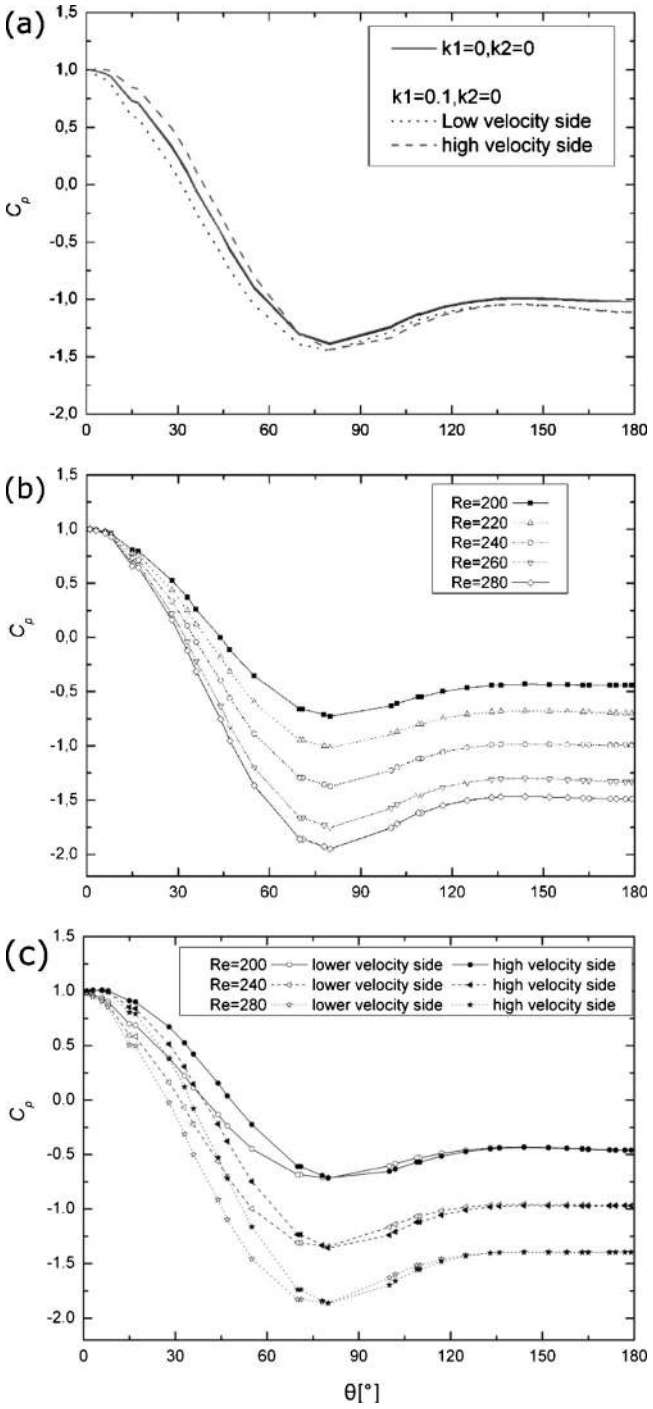

FIG. 6. Distribution of the mean pressure coefficient C_p on the surface of the cylinder: (a) uniform inflow ($k1=0$, $k2=0$) and planar shear ($k1=0.1$, $k2=0$), (b) spanwise shear, and (c) bidirectional shear.

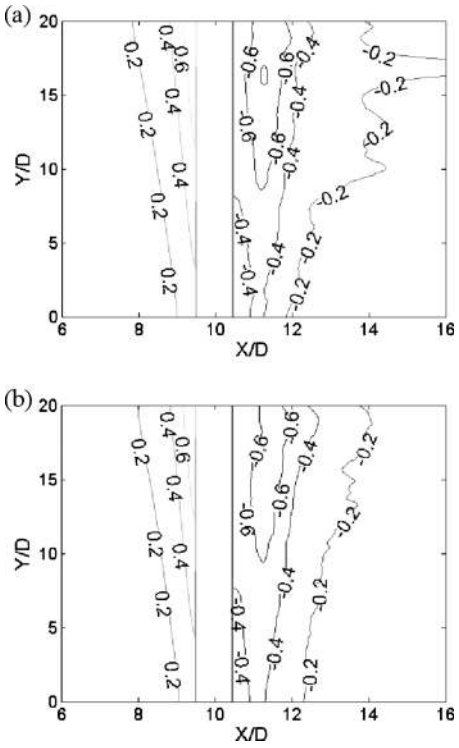

FIG. 7. Mean pressure ($\bar{P}/\rho U_o^2$) contours in the X-Y section plane through the axis of the cylinder. The cylinder is drawn as bold lines with the axis at $X/D=10$: (a) spanwise shear and (b) bidirectional shear.

sponding uniform inflow study. From Table I, it can be observed that the Reynolds numbers used in Refs. 13, 14, and 16 are extremely high when compared to the present study, and their wake flow was in the turbulent regime, while the present wake is in the transition regime. It is likely that the effect of planar shear inflow differs between high and low Reynolds number flows.

Figure 6(b) illustrates the distribution of C_p at different spanwise locations identified by the local Reynolds number Re along the span for the current spanwise shear case. At the median Reynolds number Re=240, it is surprising to see that the base pressure coefficient −1.0 matches the base pressure value from the present uniform inflow case. Nevertheless, the significant base pressure gradient along the span in the spanwise shear case should be noted. Such a spanwise variation of the base pressure was also reported in the high Reynolds number turbulence experiments of Rooney and Peltzer[20] and Woo *et al.*[21] and in the laminar flow studies of Mukhopadhyay *et al.*[24,25] In the present study, the base pressure values are quantified in the wake transition regime. In Fig. 6(c), the C_p variations from the bidirectional shear case are presented. Here, the combined effect of the planar shear and the spanwise shear on C_p can be observed. The C_p distribution on the high and low-velocity sides at three spanwise cross sections departs and is similar to the present planar shear data up to about 70°. Thereafter, the data collapse along the after-body, i.e., on the lee-side of the cylinder. At $\theta=180°$, again we see a spanwise base pressure gradient being set up. Upon comparing the base pressure gradient in Figs. 6(b) and 6(c), it can be inferred that the addition of planar shear to the spanwise shear inflow produces only modest variations in the base pressure coefficient.

The mean pressure contours (isobars) in Figs. 7(a) and 7(b), i.e., from both the spanwise shear case and the bidirectional shear case, respectively, show that the isobars are inclined to the cylinder axis, thereby giving rise to a spanwise pressure gradient, both upstream and downstream the uniform cylinder. If we now look into Fig. 8, it can be observed that this spanwise pressure gradient is driving a mean secondary flow along the span in both cases. It can be noted

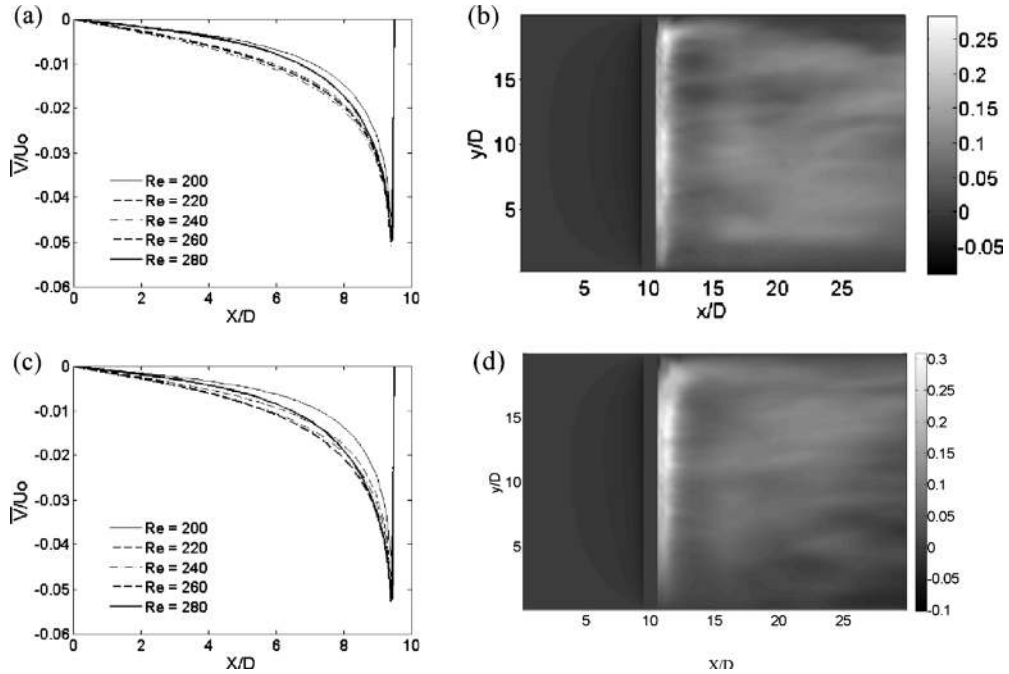

FIG. 8. Time-mean spanwise velocity $\bar{V}/U_o$ (secondary flow) along the span: [(a) and (c)] at some different spanwise locations identified by the local Reynolds number; [(b) and (d)] velocity contours in the X-Y section plane through the axis of the cylinder. The axis of the cylinder is at $X/D=10$: (a) spanwise shear: upstream the cylinder, (b) spanwise shear, (c) bidirectional shear: upstream the cylinder, and (d) bidirectional shear.

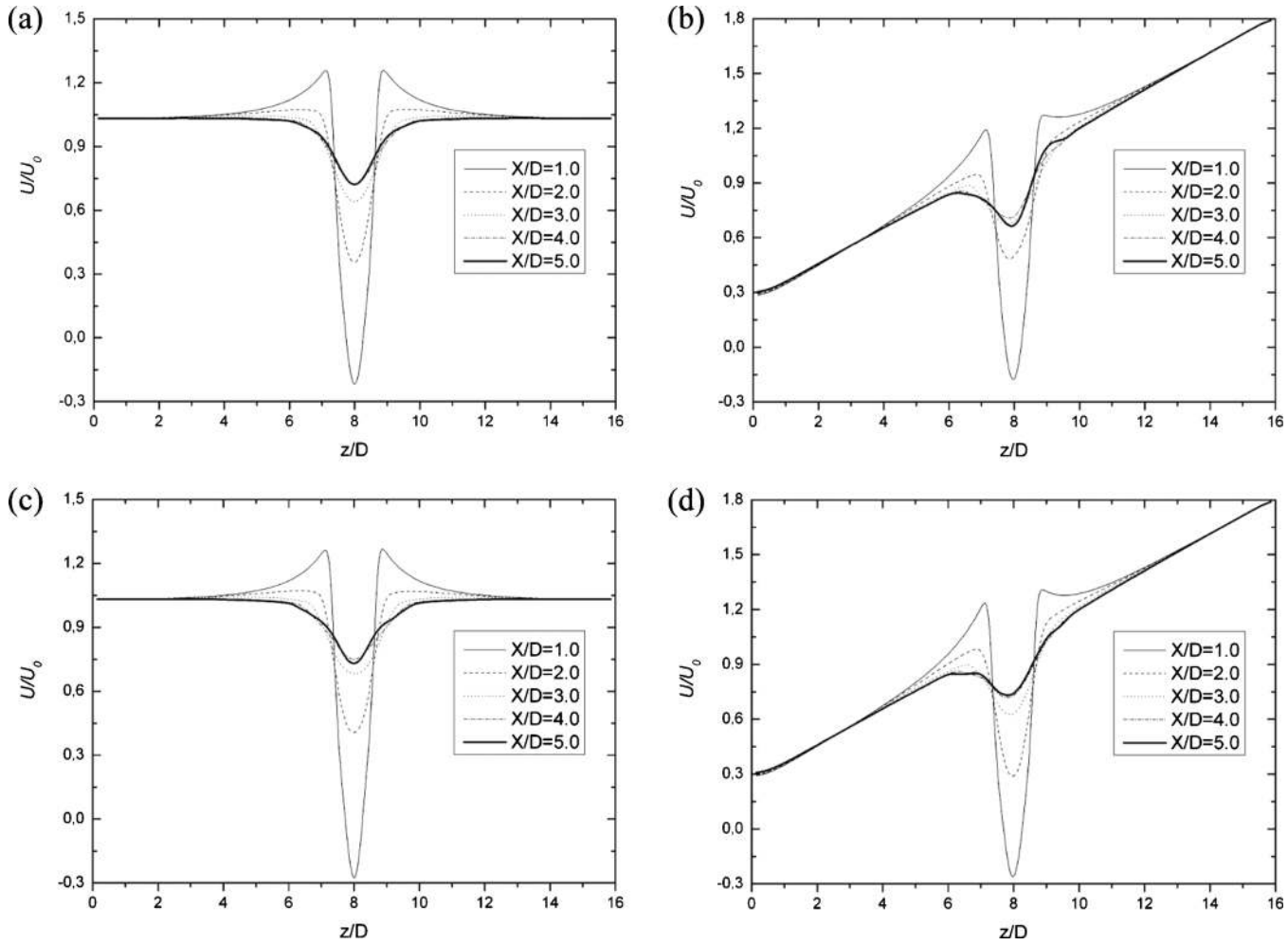

FIG. 9. Mean streamwise velocity ($\bar{U}/U_o$) profiles at fixed X/D positions (measured from the axis of the cylinder): (a) uniform inflow, (b) planar shear, (c) spanwise shear, and (d) bidirectional shear.

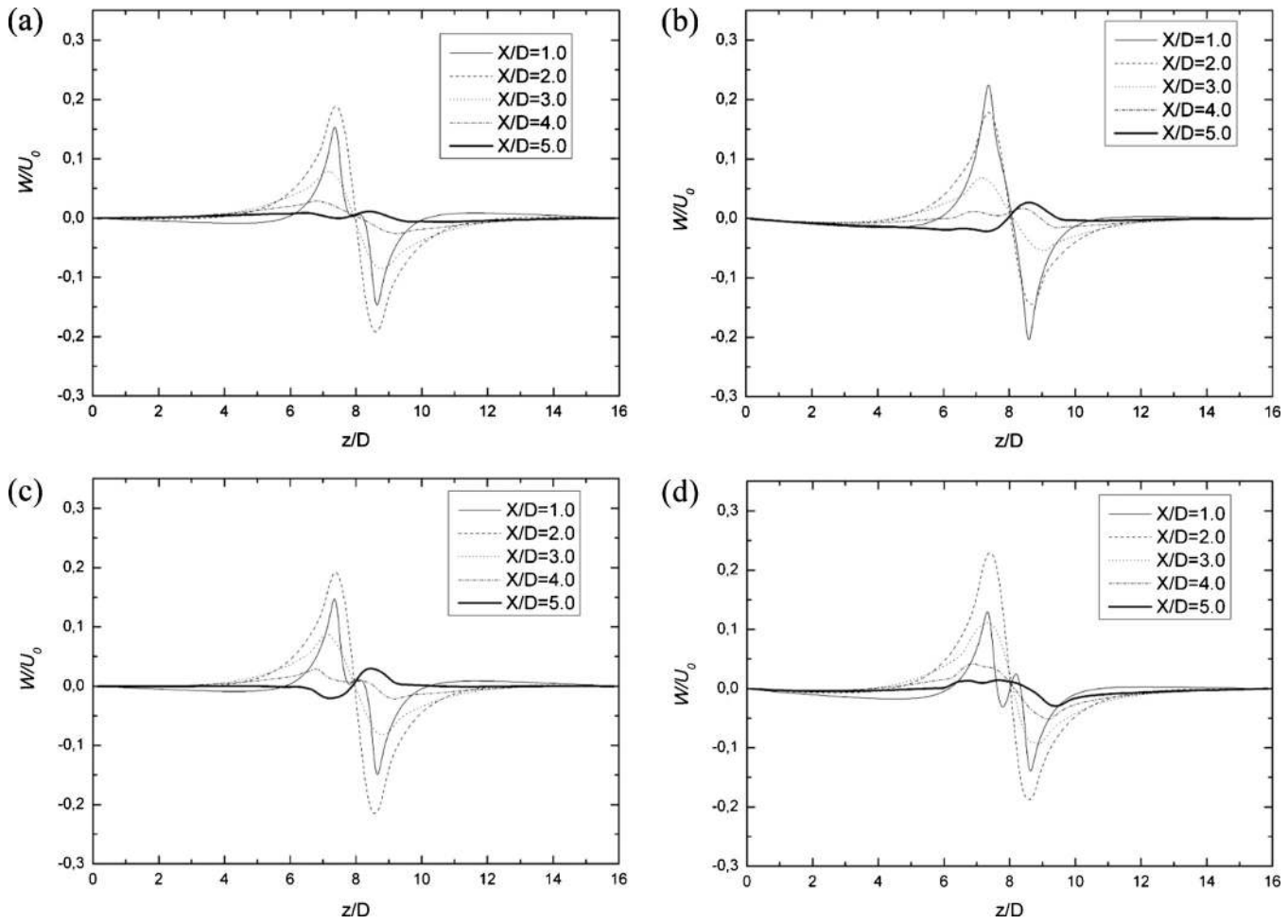

FIG. 10. Mean cross-stream velocity ($\bar{W}/U_o$) profiles at fixed X/D positions (measured from the axis of the cylinder): (a) uniform inflow, (b) planar shear, (c) spanwise shear, and (d) bidirectional shear.

from Figs. 8(a) and 8(c) that in the front stagnation zone the secondary flow $\bar{V}$ goes from the high-velocity end (Re_h =300) to the low-velocity end (Re_l=180). The magnitude of this spanwise velocity is modest, around 5% of the median velocity U_o. On the contrary, the secondary motion on the lee-side of the cylinder goes in the opposite direction in both cases [see Figs. 8(b) and 8(d)]. The magnitude of this spanwise velocity is typically of the order of 25%–30% of the median velocity U_o. The characteristics of secondary motion in the present spanwise shear case are in excellent agreement with the experimental findings of Woo *et al.*,[21] although they found a slightly higher magnitude of about 44% of their mean flow velocity. This is most likely due to their high Reynolds numbers and higher shear parameter $k2$ than in the present study (see Table I). If we now compare Fig. 8(b) with Fig. 8(d), it is interesting to note that combining the planar shear and spanwise shear together produces slightly more pronounced secondary motion. It is worth mentioning here that secondary motion has been observed recently by Narasimhamurthy *et al.*[29] in the wake transition behind a tapered circular cylinder. In that case, however, they attributed the driving mechanism of the secondary flow to the intrinsic secondary instabilities rather than the spanwise pressure gradient.

D. Reynolds-averaged statistics

The unsteady flow field can conveniently be decomposed into mean and fluctuating parts analogous to the Reynolds decomposition of a fully turbulent flow field. Here, however, the unsteadiness in the present cases is associated with the quasiperiodic vortex shedding and vortex instabilities developing in the wake flow. The cross-stream variations of the mean velocity components $\bar{U}$ and $\bar{W}$ at midspan $Y=10D$ are shown in Figs. 9 and 10, respectively. The velocity defect, i.e., momentum deficit, in the near wake is gradually reduced with increasing downstream distance X in all four cases. While the wake is symmetric in the presence of spanwise shear in Fig. 9(c), the incoming planar shear inevitably makes the wake profile asymmetric in Figs. 9(b) and 9(d). The velocity overshoot due to the blocking of the cylinder is about 20% and slightly higher at the upper side of the cylinder where the oncoming flow is faster. It is noteworthy that the velocity defect in the bidirectional shear case is larger than in the planar shear case, although the velocity profiles exhibit the same shape. This is probably due to the excess mixing caused by three-dimensionalization induced by the spanwise shear, as shown in Fig. 2.

The profiles of the cross-stream mean velocity compo-

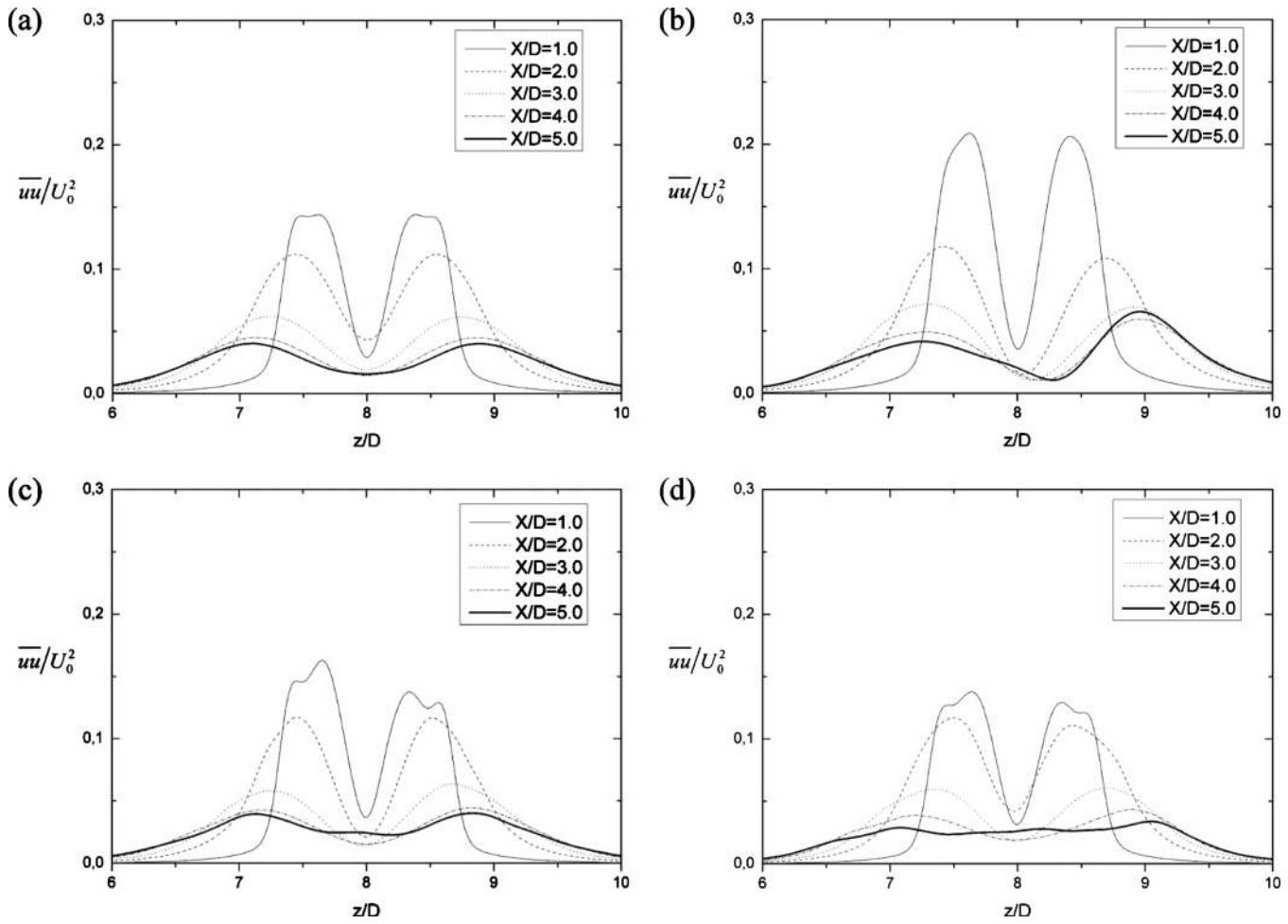

FIG. 11. Profiles of $\overline{uu}/U_o^2$ at fixed X/D positions (measured from the axis of the cylinder: (a) uniform inflow, (b) planar shear, (c) spanwise shear, and (d) bidirectional shear.

nent $\bar{W}$ in Fig. 10 are antisymmetric about the midplane $Z/D=8.0$ in the absence of planar shear. The mean motion is directed toward the midplane since $\bar{W}>0$ for $Z/D<8$ and $\bar{W}<0$ for $Z/D>8$. The antisymmetric variation is broken in the presence of planar shear but the $\bar{W}$-profiles are still surprisingly close to being antisymmetric. In the very-near-wake at $X/D=1.0$ in Fig. 10(d), $\bar{W}$ is directed away from the midplane. This flow reversal is the signature of tiny recirculation cells formed in the base region as a result of the bidirectional shear.

The variations of the second moments $\overline{uu}$ and $\overline{ww}$ are shown in Figs. 11 and 12, respectively. The bimodal distribution of $\overline{uu}$ and the monomodal variation of $\overline{ww}$ resemble the Reynolds-averaged results by Persillon and Braza[10] for a cylinder wake and those of Narasimhamurthy and Andersson[37] for a normal flat plate. In the presence of planar shear, the profiles of $\overline{uu}$ in Fig. 11(b) become increasingly asymmetric with downstream distance and exhibit substantially higher values at the high-speed side of the cylinder. The fluid shed from the upper side of the cylinder carries vorticity of the same sign as the incoming shear flow and is therefore likely to be promoted, whereas vortices shed from the lower side of the cylinder rotate oppositely to the oncoming fluid elements. The inclusion of spanwise shear, however, suppresses this tendency, and the profiles of $\overline{uu}$ and $\overline{ww}$ for the bidirectional shear case closely resemble those from the spanwise shear case. In fact, the profiles in Figs. 11(d) and 12(d) are quantitatively and qualitatively different from those in the planar shear case.

In the present Reynolds number range, the major contribution to the second moments shown in Figs. 11 and 12 is from the quasiperiodic vortex shedding. While the presence of a planar shear breaks the symmetry of the vortex shedding, a spanwise shear tends to increase the three-dimensionalization of the wake. It is noteworthy that the asymmetries resulting from a planar shear alone have been opposed by the inclusion of spanwise shear in the combined, i.e., bidirectional, shear case. It can be inferred that the three-dimensionalization due to spanwise shear tends to restore the wake symmetry. The profiles for the bidirectional shear case in Figs. 11(d) and 12(d) closely resemble those of the spanwise shear case. The shedding appears to be more symmetric and at the same time less energetic than in the planar shear case. This observation is consistent with the snapshots of the wake topology in Figs. 4 and 5. Although oblique shedding is observed both in the spanwise shear case and the bidirec-

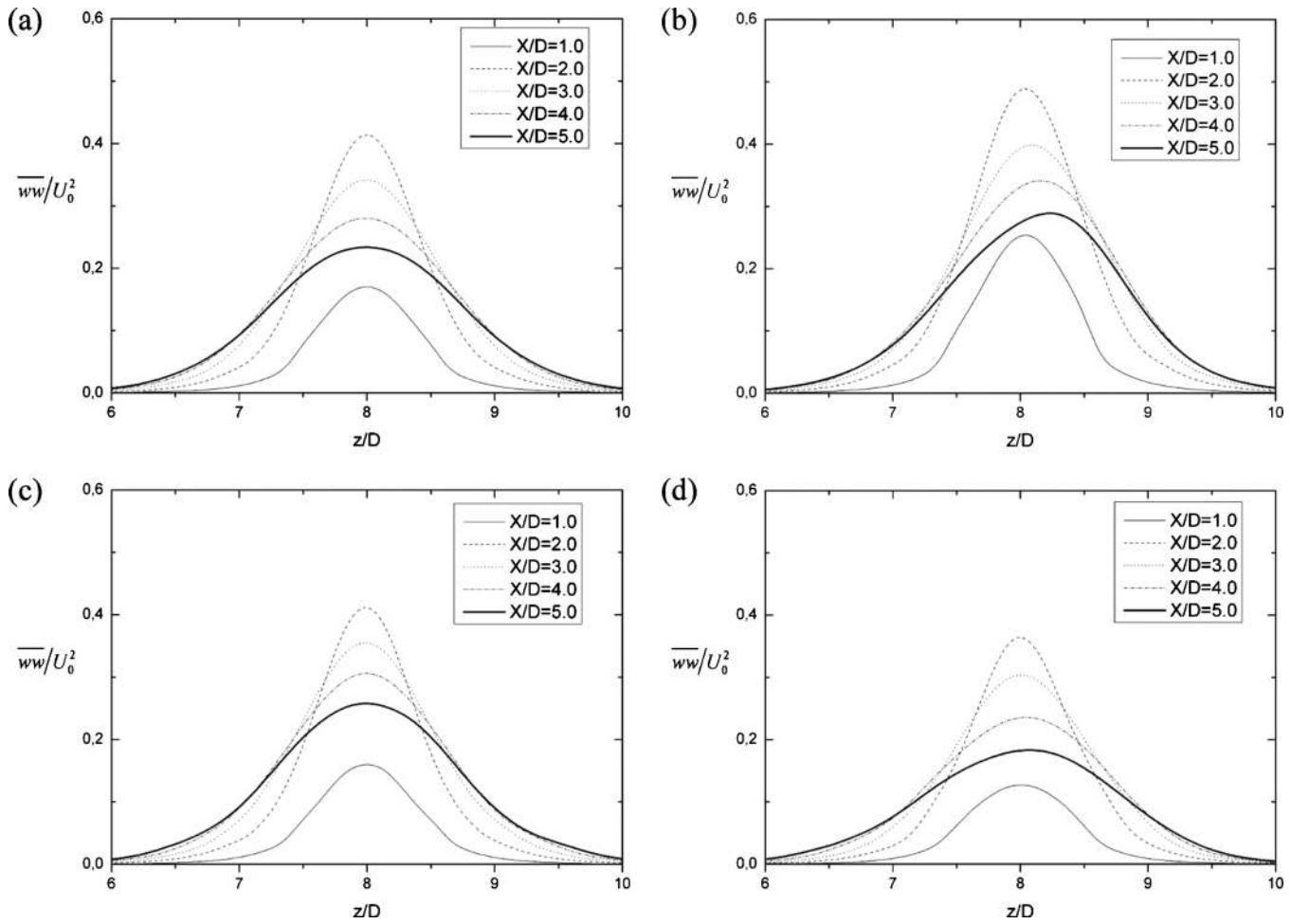

FIG. 12. Profiles of $\overline{ww}/U_o^2$ at fixed X/D positions (measured from the axis of the cylinder): (a) uniform inflow, (b) planar shear, (c) spanwise shear, and (d) bidirectional shear.

tional shear case, the shed vortex cells in the latter case are severely distorted by the presence of planar shear and the cells are also less energetic.

IV. CONCLUDING REMARKS

In the present manuscript, results from computer simulations of wake flow behind a circular cylinder in a bidirectional shear flow have been reported. The results were compared with the results for three other inflow cases: a uniform inflow, an inflow with shear across the cylinder, and an inflow with shear along the span. When the inflow velocity varied linearly across the cylinder, the associated constant vorticity was parallel with the cylinder axis, whereas in the case with a spanwise variation of the oncoming velocity, the vorticity vector was perpendicular not only to the velocity but also to the cylinder axis. In the present case with bidirectional shear inflow, the constant inflow vorticity vector was also at a right angle to the velocity vector, but inclined relative to the cylinder axis.

The presence of planar shear tends to increase the length of the shedding cells as compared with the case with only spanwise shear. The cells now exceed the limiting length of about 5 diameters reported by Griffin.[17] The presence of a planar shear alone gave rise to asymmetric variations of the mean flow components and the second moments of the velocity fluctuations across the flow. The inclusion of a spanwise shear turned out to almost eliminate this tendency. Vortex splitting and the cellular shedding induced by the spanwise shear component apparently provided sufficient three-dimensional scrambling to outweigh the effect of the planar shear. The second-moment statistics in the bidirectional shear case therefore closely resembled the results from the spanwise shear case even though the planar shear was four times the spanwise shear component.

It was indeed remarkable to observe that the shed vortex cells became less energetic in the presence of bidirectional shear than in planar shear alone. This phenomenon is associated with vortex stretching and tilting caused by the inclusion of the spanwise shear component, which tend to randomize the otherwise planar vortex shedding. It can therefore be conjectured that the cylinder wake in bidirectional shear flow will become turbulent at a lower Reynolds number than in a planar shear flow.

The present study has been restricted to a median Reynolds number 240 in the transitional regime. However, cellular vortex shedding is known to exist also at higher Reynolds numbers when the wake is turbulent (see, e.g., Ref. 33). It can therefore be anticipated that the competition

between wake asymmetries due to planar shear and three-dimensionalization due to spanwise shear will prevail also at higher Reynolds numbers. In the turbulent flow regime, however, the three-dimensional turbulence will tend to make the cellular shedding less pronounced and only a qualitative correspondence with the present findings should therefore be expected.

ACKNOWLEDGMENTS

The first authors are grateful to The Research Council of Norway for their financial support. This work has also been supported by The Research Council of Norway (Programme for Supercomputing) through a grant of computing time.

[1] M. M. Zdravkovich, *Flow Around Circular Cylinders* (Oxford University Press, Oxford, 1997), Vol. 1.
[2] C. H. K. Williamson, "The existence of two stages in the transition to three-dimensionality of a cylinder wake," Phys. Fluids **31**, 3165 (1988).
[3] C. H. K. Williamson, "The natural and forced formation of spot-like vortex dislocations in the transition of a wake," J. Fluid Mech. **243**, 393 (1992).
[4] H. Zhang, U. Fey, B. R. Noak, M. König, and H. Eckelmann, "On the transition of the cylinder wake," Phys. Fluids **7**, 779 (1995).
[5] R. Mittal and S. Balachandar, "Generation of streamwise vortical structures in bluff body wakes," Phys. Rev. Lett. **75**, 1300 (1995).
[6] C. H. K. Williamson, "Three-dimensional wake transition," J. Fluid Mech. **328**, 345 (1996).
[7] D. Barkley and R. D. Henderson, "Three-dimensional Floquet stability analysis of the wake of a circular cylinder," J. Fluid Mech. **322**, 215 (1996).
[8] M. Thompson, K. Hourigan, and J. Sheridan, "Three-dimensional instabilities in the wake of a circular cylinder," Exp. Therm. Fluid Sci. **12**, 190 (1996).
[9] C. H. K. Williamson, "Vortex dynamics in the cylinder wake," Annu. Rev. Fluid Mech. **28**, 477 (1996).
[10] H. Persillon and M. Braza, "Physical analysis of the transition to turbulence in the wake of a circular cylinder by three-dimensional Navier-Stokes simulation," J. Fluid Mech. **365**, 23 (1998).
[11] M. Kiya, H. Tamura, and M. Arie, "Vortex shedding from a circular cylinder in moderate-Reynolds-number shear flow," J. Fluid Mech. **101**, 721 (1980).
[12] T. S. Kwon, H. J. Sung, and J. M. Hyun, "Experimental investigation of uniform-shear flow past a circular cylinder," ASME Trans. J. Fluids Eng. **114**, 457 (1992).
[13] D. Sumner and O. O. Akosile, "On uniform planar shear flow around a circular cylinder at subcritical Reynolds number," J. Fluids Struct. **18**, 441 (2003).
[14] S. Cao, S. Ozono, K. Hirano, and Y. Tamura, "Vortex shedding and aerodynamic forces on a circular cylinder in linear shear flow at subcritical Reynolds number," J. Fluids Struct. **23**, 703 (2007).
[15] C. Lei, L. Cheng, and K. Kavanagh, "A finite difference solution of the shear flow over a circular cylinder," Ocean Eng. **27**, 271 (2000).
[16] T. Omori, S. Jakirlić, C. Tropea, and S. Obi, "Shearless and sheared flow past a circular cylinder: Comparative analysis by means of LES," Int. J. Heat Fluid Flow **29**, 703 (2008).
[17] O. M. Griffin, "Vortex shedding from bluff bodies in a shear flow: A review," ASME Trans. J. Fluids Eng. **107**, 298 (1985).
[18] W. A. Mair and P. K. Stansby, "Vortex wakes of bluff cylinders in shear flow," SIAM J. Appl. Math. **28**, 519 (1975).
[19] S. Tavoularis, H. Stapountzis, and U. Karnik, "Vortex shedding from bluff cylinders in strongly sheared turbulent streams," J. Wind. Eng. Ind. Aerodyn. **26**, 165 (1987).
[20] D. M. Rooney and R. D. Peltzer, "Pressure and vortex shedding patterns around a low aspect ratio cylinder in a sheared flow at transitional Re," ASME Trans. J. Fluids Eng. **103**, 88 (1981).
[21] H. G. C. Woo, J. A. Peterka, and J. E. Cermak, "Secondary flows and vortex formation around circular cylinder in constant shear flow," J. Fluid Mech. **204**, 523 (1989).
[22] M. Kappler, W. Rodi, S. Szepessy, and O. Badran, "Experiments on the flow past long circular cylinders in a shear flow," Exp. Fluids **38**, 269 (2005).
[23] J. H. Silvestrini and E. Lamballais, "Direct numerical simulation of oblique vortex shedding from a cylinder in shear flow," Int. J. Heat Fluid Flow **25**, 461 (2004).
[24] A. Mukhopadhyay, P. Venugopal, and S. P. Vanka, "Numerical study of vortex shedding from a circular cylinder in linear shear flow," ASME Trans. J. Fluids Eng. **121**, 460 (1999).
[25] A. Mukhopadhyay, P. Venugopal, and S. P. Vanka, "Oblique vortex shedding from a circular cylinder in linear shear flow," Comput. Fluids **31**, 1 (2002).
[26] A. Lankadasu and S. Vengadesan, "Onset of vortex shedding in planar shear flow past a square cylinder," Int. J. Heat Fluid Flow **29**, 1054 (2008).
[27] P. Parnaudeau, D. Heitz, E. Lamballais, and J. H. Silvestrini, "Direct numerical simulations of vortex shedding behind cylinders with spanwise linear nonuniformity," J. Turbul. **13** (2007).
[28] V. D. Narasimhamurthy, H. I. Andersson, and B. Pettersen, "Steady viscous flow past a tapered cylinder," Acta Mech. **206**, 53 (2009).
[29] V. D. Narasimhamurthy, H. I. Andersson, and B. Pettersen, "Cellular vortex shedding behind a tapered circular cylinder," Phys. Fluids **21**, 044106 (2009).
[30] M. Manhart, "A zonal grid algorithm for DNS of turbulent boundary layers," Comput. Fluids **33**, 435 (2004).
[31] R. N. Kieft, C. C. M. Rindt, A. A. van Steenhoven, and G. J. F. van Heijst, "On the wake structure behind a heated horizontal cylinder in cross-flow," J. Fluid Mech. **486**, 189 (2003).
[32] N. Peller, A. Le Duc, F. Tremblay, and M. Manhart, "High-order stable interpolations for immersed boundary methods," Int. J. Numer. Methods Fluids **52**, 1175 (2006).
[33] V. D. Narasimhamurthy, H. I. Andersson, and B. Pettersen, "Cellular vortex shedding in the wake of a tapered plate," J. Fluid Mech. **617**, 355 (2008).
[34] C. H. K. Williamson and A. Roshko, "Measurements of base pressure in the wake of a cylinder at low Reynolds numbers," Z. Flugwiss. Weltraumforsch. **14**, 38 (1990).
[35] C. Norberg, "An experimental investigation of the flow around a circular cylinder: Influence of aspect ratio," J. Fluid Mech. **258**, 287 (1994).
[36] H. A. Khaledi, M. Barri, and H. I. Andersson, "On the stabilizing effect of the Coriolis force on the turbulent wake of a normal flat plate," Phys. Fluids **21**, 095104 (2009).
[37] V. D. Narasimhamurthy and H. I. Andersson, "Numerical simulation of the turbulent wake behind a normal flat plate," Int. J. Heat Fluid Flow **30**, 1037 (2009).